Journal of Molecular Catalysis A: Chemical 327 (2010) 101–109

Contents lists available at ScienceDirect

Journal of Molecular Catalysis A: Chemical

journal homepage: www.elsevier.com/locate/molcata

Photoinduced formation of reactive oxygen species in suspensions of titania mechanochemically synthesized from $TiCl_4$

Vlasta Brezová[a,*], Peter Billik[b,c], Zuzana Vrecková[a], Gustav Plesch[b]

[a] Institute of Physical Chemistry and Chemical Physics, Faculty of Chemical and Food Technology, Slovak University of Technology in Bratislava, Radlinského 9, SK-812 37 Bratislava, Slovak Republic
[b] Faculty of Natural Sciences, Comenius University, Mlynská dolina, SK-842 15 Bratislava, Slovak Republic
[c] Department of Magnetometry, Institute of Measurement Science, Slovak Academy of Sciences, Dúbravská cesta 9, SK-841 04 Bratislava, Slovak Republic

ARTICLE INFO

Article history:
Received 19 March 2010
Received in revised form 28 April 2010
Accepted 26 May 2010
Available online 2 June 2010

Keywords:
Titanium dioxide
Anatase
Mechanochemical synthesis
EPR spectroscopy
Spin trapping
Nitroxide radicals

ABSTRACT

Titanium dioxide nanopowders were synthesized mechanochemically using $TiCl_4$ and $(NH_4)_2CO_3$ (series **TC**) or $TiCl_4/(NH_4)_2CO_3$ and Na_2SO_4–$Na_2SO_4{\cdot}10H_2O$ (series **TCSM**), as precursors and post-annealing in the temperature range 150–850 °C. Crystal structure and crystallite size of the titania nanomaterials were characterized by X-ray diffraction, and the optical properties of aqueous suspensions at various TiO_2 loadings were measured using UV/visible spectroscopy. The photoinduced activity was measured *in situ* by EPR spectroscopy applying a variety of experimental techniques (spin trapping, spin probes, 4-hydroxy-2,2,6,6-tetramethylpiperidine oxidation). In the series **TC** the presence of an NH_4Cl salt matrix, which was removed by decomposition to gaseous byproducts in the post-annealing process, leads to the formation of anatase nanocrystals with optimal size for high photoactivity (23–50 nm) at temperatures of 550 and 650 °C, and these titania samples are the most active in the photoinduced production of reactive oxygen species. The results found for **TCSM** series confirmed that the presence of a sulfate salt matrix (Na_2SO_4) during mechanochemical and annealing processes significantly hindered TiO_2 nanocrystallite growth, increased agglomerate formation in aqueous media and lowered the values of photonic efficiencies determined *via* paramagnetic species formation or termination.

1. Introduction

The unique physicochemical properties of titanium dioxide polymorphs (anatase, brookite, rutile) and their ability to produce, upon UVA photoexcitation, electron (e^-) and hole (h^+) pairs leading to consecutive chemical reactions, represent topics of intensive multidisciplinary research [1–5]. The photoactivity of TiO_2 is determined by the processes of electron/hole pair formation, recombination, interfacial transfer of charge carriers and their surface reactions with the adsorbed species [3,6–8]. These processes are substantially influenced by the titania crystal structure, particle size, morphology and porosity [1,2,4,6,9–11]. Photogenerated holes may be trapped on lattice oxide ions forming O^-anions or hydroxyl radicals (•OH) [9,12–14]. Alternatively, h^+ may react with adsorbed water molecules or hydroxide anions producing •OH, or directly oxidize adsorbed organic/inorganic substrates [3,15,16]. In oxygenated systems the photogenerated electrons are scavenged by molecular oxygen, producing super oxide radical anions [17–19], which may act as oxidizing agents or as an additional source of hydroxyl radicals *via* the consequent formation of hydrogen peroxide [9,20]. The processes involved in the formation of paramagnetic species upon photoexcitation of titania materials have been intensively investigated by EPR spectroscopy using different experimental techniques [12,18–23].

The environmental applications of TiO_2 (photoinduced removal of pollutants from water and air) require effective production of Reactive Oxygen Species (ROS; e.g. •OH, $^{\bullet}OOH/O_2^{\bullet-}$, H_2O_2, $^1O_2$) during irradiation [3,4]. On the other hand, for the applications of titania nanoparticles in the cosmetic industry, TiO_2 photoactivity is undesirable and, it is necessary to suppress photoinduced ROS generation completely [19]. Consequently, considerable attention is focused on the synthesis, physicochemical and photochemical characterization of TiO_2 in order to prepare specific titania materials with the required properties [4,24–29].

Abbreviations: ABTS, 2,2′-azino-bis(3-ethylbenzothiazoline-6-sulfonate) diammonium salt; ACN, acetonitrile; DABCO, 1,4-diazabicyclo[2.2.2]octane; DMPO, 5,5-dimethyl-1-pyrroline *N*-oxide; DPPH, 1,1-diphenyl-2-picrylhydrazyl; E_{bg}, band-gap energy; EPR, electron paramagnetic resonance; FWHM, full widths at half-maximum; POBN, α-(4-pyridyl-1-oxide) *N*-*tert*-butylnitrone; ROS, reactive oxygen species; SW, magnetic field sweep width; TMP, 4-hydroxy-2,2,6,6-tetramethylpiperidine; TEMPOL, 4-hydroxy-2,2,6,6-tetramethylpiperidine *N*-oxyl; UV/vis, ultraviolet/visible; XRD, X-ray diffraction.

* Corresponding author. Tel.: +421 2 5932 5666; fax: +421 2 5292 6032.
E-mail address: vlasta.brezova@stuba.sk (V. Brezová).

1381-1169/$ – see front matter © 2010 Elsevier B.V. All rights reserved.
doi:10.1016/j.molcata.2010.05.019

In recent years, in addition to the more popular solution and gas-phase techniques for preparation of titanium dioxide nanopowders (sol–gel and microemulsion procedures, hydrothermal synthesis, coprecipitation, flame hydrolysis, etc.), increased attention has been devoted to mechanochemical synthesis of TiO_2 [30–36]. In the high-energy milling process amorphous titanium dioxide is formed by the reaction of suitable precursors. The activation energy is provided by transformation of energy from the milling bodies to the milled powder. The presence of water in the reaction system enhances the reaction and it can be assumed that in this case the reaction conditions in high-energy milling show some similarity with hydrothermal conditions [30,32,34]. The byproducts formed are usually a soluble salt matrix, which is removed after the annealing process by washing in an appropriate solvent. The nanocrystalline TiO_2 product is formed in an annealing process at a suitable temperature. The presence of the salt matrix during the milling and post-annealing processes allows the preparation of nanopowders with a relatively small degree of hard association. The use of $TiCl_4$ as a reaction precursor for mechanochemical synthesis of titanium dioxide was firstly reported by Billik et al. [31,36], and it was shown that its application has an advantage in that a subsequent washing of the byproduct NH_4Cl is not necessary, since it decomposes and evolves in the form of gaseous products in the post-annealing reaction [31].

The aim of this paper is a detailed photoactivity investigation of TiO_2 nanopowders prepared mechanochemically from $TiCl_4$. The synthesized titania nanomaterials were characterized by their crystal structure, optical properties in aqueous suspensions and photonic efficiency in the formation of reactive oxygen species evaluated from data monitored by *in situ* EPR spectroscopy using various experimental techniques.

2. Experimental

2.1. Chemicals and reagents

Two series (**TC** and **TCSM**) of mechanochemically synthesized TiO_2 samples were investigated.

Nanopowders in the series **TC** were prepared by mechanochemical synthesis using, as precursors, $TiCl_4$ (Fluka, >98%; 3 cm^3) and $(NH_4)_2CO_3$ (Lachema, Czech Republic; 7.9 g) corresponding to the molar ratio 1:3. The reaction was performed in a high-energy ball mill TB-1 (Kadaň, Ltd., Slovak Republic) using corundum jars at milling speeds of 890 rpm for 5 min. The synthesized powders representing non-crystalline hydrated TiO_2 were subsequently annealed in the temperature range of 150–850 °C. A heating rate of 10 °C min^{-1} was used. Titania samples in the series **TCSM** were prepared by a 3-min milling of $TiCl_4$ (3 cm^3) and $(NH_4)_2CO_3$ (5.25 g), i.e., in molar ratio 1:2, to which Na_2SO_4 (Lachema, Czech Republic; 2 g) and $Na_2SO_4{\cdot}10\ H_2O$ (Lachema, Czech Republic; 2 g) were added. The prepared white solids were subsequently annealed in the range of 350–850 °C, then dispersed by ultrasound in hot water for 1 min to remove water-soluble Na_2SO_4, and finally washed and dried at 120 °C [31]. An overview of the samples investigated is given in Table 1.

The commercial photoactive titanium dioxide Aeroxide® P25 was kindly provided by Evonik Degussa (Germany). The TiO_2 stock suspensions (1×10^{-3} g cm^{-3}) were prepared by sonication (Ultrasonic Compact Cleaner TESON 1, Tesla, Slovak Republic) in either distilled water or acetonitrile (ACN; SeccoSolv® Merck).

The spin trapping agent, 5,5-dimethyl-1-pyrroline *N*-oxide (DMPO; Aldrich) was distilled before application and stored under argon, α-(4-pyridyl-1-oxide) *N*-*tert*-butylnitrone (POBN; Aldrich) was used without purification. The concentration of photogenerated spin-adducts was determined using aqueous solutions of 4-hydroxy-2,2,6,6-tetramethylpiperidine *N*-oxyl (TEMPOL; Aldrich) as calibration standards. As sources of semi-stable free radicals TEMPOL and the radical cation of 2,2′-azino-bis(3-ethylbenthiazoline-6-sulfonate) ($ABTS^{\bullet+}$) prepared by oxidation of ABTS (Sigma) with $K_2S_2O_8$ (Aldrich) [20] were used. The oxidation of diamagnetic 4-hydroxy-2,2,6,6-tetramethylpiperidine (TMP; Merck-Schuchardt) to paramagnetic nitroxide radical TEMPOL was monitored by *in situ* EPR upon irradiation of titania in ACN suspensions.

2.2. Methods and apparatus

2.2.1. X-ray powder diffraction

The prepared powders were characterized by X-ray powder diffraction (XRD) using a Philips PW 1050 diffractometer and Cu Kα radiation. Crystallite sizes (D) were calculated by X-ray line broadening using the Scherrer's equation [24,31]:

$$D = \frac{0.9\lambda}{B\cos\theta} \quad B = B_s - B_m \tag{1}$$

where D is the crystallite size, λ the wavelength of the X-ray radiation (0.15418 nm), B_s is the full width at half-maximum height (FWHM) of the (1 0 1) anatase diffraction peak of the sample in radians. θ is the diffraction peak position of the sample. For the correction of the instrumental peak-broadening (B_m), the (0 1 2) diffraction of the α-Al_2O_3 standard calcined at 1500 °C has been used [37]. The fraction of the rutile phase in the powder was calculated according to the ref. [24,38], by using the integrated XRD intensities of the anatase (1 0 1) and rutile (1 1 0) peak.

2.2.2. UV/vis experiments

UV/visible spectra of aqueous titania suspensions were recorded using a UV-3600 UV/vis spectrometer (Shimadzu, Japan) with a large integrating sphere assembly with a transmittance measurement accessory (1 cm square quartz cell). The freshly prepared titania suspensions with low concentrations (1×10^{-5}–1×10^{-4} g cm^{-3}) were sonicated for 1 min and then the UV/vis spectra were measured in duplicate. The values of absorption and scattering coefficients in the wavelength interval 240–600 nm ($\Delta\lambda$ = 5 nm) were evaluated from the experimental extinction data by a least-squares minimization procedure using the Kubelka–Munk model [39–41].

2.2.3. EPR in situ photochemical experiments

Titania suspensions containing spin trapping agents (DMPO and POBN), semi-stable paramagnetic species (TEMPOL and $ABTS^{\bullet+}$), or TMP were prepared directly before the EPR measurements. The stock TiO_2 suspension (1×10^{-3} g cm^{-3}) was homogenized in an ultrasonic bath for 1 min prior to the addition of agents and diluted to a final titania concentration of 5×10^{-4} g cm^{-3}. The suspensions were then carefully mixed by a slight air stream and immediately transferred to a small quartz flat cell (WG 808-Q, Wilmad-LabGlass, USA; optical cell length 0.045 cm) optimized for the TE_{102} cavity of an EMX X-band EPR spectrometer (Bruker, Germany). The samples were irradiated at 295 K directly in the EPR resonator and the EPR spectra were recorded *in situ*. As an irradiation source an HPA 400/30S lamp (400 W, Philips, λ_{max} = 365 nm [42]) was used. The UVA irradiance of the radiation source within the EPR cavity (2.7 mW cm^{-2} or 5.5 mW cm^{-2} after lamp replacement) was determined using a UV Light Meter UV-340, Lutron (Lutron Ltd., UK) and UVX radiometer (UVP, USA), respectively. A Pyrex glass filter (with a thickness of 1 mm) was used to eliminate radiation wavelengths below 300 nm. The first spectrum in the time-domain was measured without radiation, and subsequently, upon continuous irradiation ten spectra were recorded. The concentration of paramagnetic species was evaluated from the double-integrated EPR

Table 1
Phase composition, mean crystallite size of anatase, extinction coefficient of aqueous suspension at λ = 365 nm, and band-gap energy of mechanochemically synthesized titania powders annealed at different temperatures. The samples are designated by a capital letters and a number, characterizing the synthesis series and the annealing temperature.

Sample	Annealing temperature (°C)	Phase composition anatase/rutile (wt%)	Mean crystallite size of anatase (nm)	$\beta^{\lambda=365}$ (cm^2 g^{-1})	E_{bg} (eV)
TC150	150	Amorphous	–	3400	–
TC200	200	Amorphous	–	6100	–
TC230	230	100/0	12	4500	3.2
TC250	250	100/0	13	8000	3.20
TC350	350	100/0	18	10,900	3.20
TC450	450	100/0	23	10,600	3.25
TC550	550	100/0	31	11,000	3.25
TC650	650	~99/1	50	9700	3.20
TC750	750	94/6	~70[a]	8700	–
TC850	850	75/25	~100[a]	2700	–
TCSM350	350	100/0	7	3900	3.20
TCSM450	450	100/0	15	2400	3.20
TCSM550	550	100/0	23	2200	3.25
TCSM650	650	~98/2	38	2100	3.20
TCSM750	750	84/16	~60[a]	1800	–
TCSM850	850	55/45	~110[a]	2900	–

[a] The calculated mean crystallite size is subjected to larger inaccuracy due to the narrow diffraction lines.

spectra using the calibration curves obtained by the EPR spectra of TEMPOL measured under identical conditions. The EPR spectra were analyzed and simulated using the Bruker software WinEPR and SimFonia and the Winsim2002 software freely available from the website of National Institute of Environmental Health Sciences (NIEHS) (http://epr.niehs.nih.gov/) [43].

The statistical analysis was carried out using the Origin (Microcal) program.

3. Results and discussion

3.1. Synthesis and characterization of TiO_2 nanopowders

The solvent-free mechanochemical synthesis of titania using $TiCl_4$ and $(NH_4)_2CO_3$ in the molar ratio 1:3 (series **TC**) led to the production of a non-crystalline network of hydrated TiO_2 and NH_4Cl as described in reaction (2) [31]:

$$TiCl_4 + 3\,(NH_4)_2CO_3 \rightarrow TiO_2{\cdot}H_2O + 4\,NH_4Cl + 3\,CO_2 + 2\,NH_3$$
$$\Delta H^{\circ} = -250\ \text{kJ mol}^{-1} \quad (2)$$

Although the reaction between $TiCl_4$ and $(NH_4)_2CO_3$ is exothermic with a large negative enthalpy change, we propose that the reaction water evolved during milling plays a crucial role in the process. This water can enhance the hydrolytic reactions of both $TiCl_4$ and $(NH_4)_2CO_3$ and thus favours the neutralization reactions of the newly formed hydrolytic products. The XRD spectra of **TC** powders annealed in the temperature range of 150–250 °C confirmed the presence of NH_4Cl diffraction together with transformation of amorphous titania to anatase nanocrystals with a crystallite size of 12–13 nm at temperatures between 230 and 250 °C (Table 1) [31]. As has been reported previously, NH_4Cl enhances the crystallization and growth process of anatase TiO_2 from its amorphous state, and nanocrystalline anatase can be prepared at temperatures as low as 250 °C, which is about 100 °C lower as it is usually found for solid state synthesis of nanopowders in bulk [44]. Low temperature synthesis of ultrafine powder nanocrystals at temperature below 200 °C can be performed, however, under solvothermal conditions [45,46]. The unusually low crystallization temperature of anatase in the case of the samples under investigation can be explained by the assistance of NH_4Cl salt matrix during annealing. However, whether the positive impact of NH_4Cl on the anatase crystallization is due to its sublimation or decomposition to HCl and NH_3, as has been proposed in Ref. [44], or that ammonium chloride assists as the salt flux during annealing process, remains an open question today.

Thermal treatment at 350 °C resulted in complete sublimation of NH_4Cl and the formation of a very voluminous anatase powder with a mean crystallite size of 18 nm (Table 1). Further increase in the annealing temperature caused the growth of anatase nanoparticles accompanied by a gradual transformation of anatase to rutile above 650 °C (Table 1).

On the other hand, the **TCSM** series was synthesized using a starting molar ratio of $TiCl_4$ and $(NH_4)_2CO_3$ of 1:2, together with the addition of Na_2SO_4 and $Na_2SO_4{\cdot}10H_2O$. The $Na_2SO_4{\cdot}10H_2O$ served as a water source to accelerate the rate of the hydrolysis of $TiCl_4$ during milling. The crystallization of anatase was observed at around 100 °C higher than in the series **TC**. The sample **TCSM**650 revealed the presence of a rutile phase at a very low concentration, and the formation of the rutile allotrope increased upon further rise of the annealing temperature (Table 1). It is well known that anatase to rutile transformation can be initiated through nucleation at the interphase between nanoparticles. Anatase is the most thermodynamically stable titania phase at sizes less than 11 nm, and rutile at greater than 35 nm [47,48]. The inhibitory effect of Na_2SO_4 on the grain growth of nanocrystalline anatase during thermal treatment was shown previously, and it was evidenced that the activation energy for the grain growth process of anatase particles was more than double in presence of Na_2SO_4 [31] when compared to the analogical reaction in absence of sodium sulfate. The presence of highly dispersed Na_2SO_4 in the salt matrix close to the anatase surface prevents effectively the direct contacts of different crystallites and thus it can prevent the crystallite growth over their critical diameter. Previously, the effect of sulfate ions on the formation of titania polymorphs, crystallite growth and photoinduced activity has been intensively investigated [28,49–53]. It has been shown that the addition of sulfate ions hindered the transformation of amorphous titania and the growth of anatase crystals [52], stabilized the anatase structure, which was transformed to rutile only in the presence of thermally decomposing residual sulfates [49–52].

The presence of surface sulfate species is proposed for samples **TCSM**350–**TCSM**650. However, in the temperature range 750–850 °C, which is close to the melting point of Na_2SO_4 ($T_m(Na_2SO_4)$ = 894 °C), the presence of Na_2SO_4 enhanced the grain growth process due to sintering processes and the transformation of anatase to rutile is thus greatly accelerated (Table 1).

In our investigations the optical properties of synthesized titania nanopowders dispersed in water were investigated by UV/vis spectroscopy under identical conditions, e.g., sonication time, scan speed.

The spectrophotometrically monitored extinction in heterogeneous titanium dioxide aqueous suspensions represents a combination of absorption and scattering caused by particles [39,41]:

$$E^{\lambda} = \beta^{\lambda} cl = (\varepsilon^{\lambda}_{abs} + \varepsilon^{\lambda}_{scat})cl \quad (3)$$

where E^{λ} is the extinction at a given wavelength λ; β^{λ} is the extinction coefficient ($cm^2\,g^{-1}$); $\varepsilon^{\lambda}_{abs}$, $\varepsilon^{\lambda}_{scat}$ are absorption and scattering coefficients ($cm^2\,g^{-1}$); c is the titanium dioxide concentration ($g\,cm^{-3}$); l is the optical path length (cm).

Fig. 1a and b shows that the addition of sulfate ions during the synthesis of **TCSM** samples caused noticeable differences in the monitored extinction spectra of aqueous suspensions in comparison to the **TC** series. The extinction values monitored for samples of **TCSM** dispersed in water are very small evidencing the formation of large agglomerates in aqueous media [54–59]. The values of the extinction coefficient determined at a wavelength of 365 nm for the synthesized samples are summarized in Table 1. Previously it has been found that the extinction coefficient of titania in aqueous suspensions significantly increased when the average agglomerate size decreased [55,56], and the size of agglomerates was affected by sonication or mixing [56]. We suggest that in the **TCSM** samples, due to existence of large amounts of water (from $Na_2SO_4{\cdot}10H_2O$), the formation of polymeric Ti–OH species, which are stable during subsequent low temperature annealing, leads to the coagulation and formation of soft agglomerates during washing. This assumption is manifested in low values of extinction (Fig. 1a and b; Table 1). Sample **TCSM**850 annealed at temperature of 850 °C resulting in the total decomposition of Ti–OH and surface sulfate species is characterized by an extinction coefficient (λ = 365 nm) of 2900 $cm^2\,g^{-1}$, compared to the value of 2700 $cm^2\,g^{-1}$ found for sample **TC**850 (Table 1). On the other hand, the high value of extinction coefficient of the **TC** samples can be explained by the use of the NH_4Cl salt matrix. In this series, where no sulfates were present, NH_4Cl decomposes, or sublimes into gaseous HCl or NH_3 upon heating, and these gaseous byproducts effectively disrupt agglomeration of the newly formed anatase particles [44]. These results are in accord with our previous results [41] where the extinction coefficients of titania samples mechanochemically prepared from a sulfate precursor were significantly lower than the value found for Aeroxide® P25 nanopowder.

The scattering characteristics of titania suspensions in ultraviolet region can significantly influence the absorption of UV radiation [39]. Consequently, the extinction spectra of titanium dioxide suspensions measured at various loadings were used to compute values of $\varepsilon^{\lambda}_{abs}$ and $\varepsilon^{\lambda}_{scat}$ (5 nm interval in the spectral region 200–600 nm) in accordance with the Kubelka–Munk model of diffuse reflectance and transmission [39,41] using a non-linear least-squares method. The calculated data were used to assemble the absorption and scattering spectra of synthesized TiO_2 samples, as shown in Fig. 1c for sample **TC**550. The calculated absorption spectra were applied in the construction of the graphical dependence of $(\varepsilon^{\lambda}_{abs}\,h\nu)^{1/2}$ on the photon energy in order to evaluate the TiO_2 band-gap energy (E_{bg}) assuming indirect transitions [41,60,61]. Fig. 1d illustrates the procedure of E_{bg} determination for sample **TC**550. Table 1 summarizes the band-gap energies calculated for the titania samples containing anatase as dominant allotrope (E_{bg} = 3.2 eV [3]).

3.2. Evaluation of photoinduced activity of TiO_2 nanopowders by in situ EPR spectroscopy

The evaluation of the photoactivity of titania nanomaterials characterized by different physical, chemical and optical properties persistently attracts the attention of researchers [5,8,12,15,17,41,62–64]. Our investigations are focused on the application of *in situ* EPR spectroscopy in the assessment of UVA photonic efficiency (ξ_{UVA}), calculated as the ratio of the initial rate of paramagnetic species transformed or formed (R_{in}) and the incident UVA photon flux (4),

$$\xi = \frac{R_{in}}{\phi^{UVA}_{inc}} \quad (4)$$

where ϕ^{UVA}_{inc} represents the incident UVA photon flux (1.8×10^{-8} Einstein s^{-1} or 3.4×10^{-8} Einstein s^{-1}, respectively).

3.2.1. Spin trapping experiments using DMPO and POBN

UVA irradiation of aqueous suspensions of synthesized TiO_2 nanopowders in the presence of a DMPO spin trap caused efficient formation of a paramagnetic species which gives rise to a four-line EPR signal (inset in Fig. 3a) characterized with spin Hamiltonian parameters a_N = 1.495 mT, $a_H{}^{\beta}$ = 1.472 mT and g-value = 2.0057, which are typical for •DMPO-OH spin-adduct [12,20,65]. The formation of hydroxyl radical spin-adducts was also evidenced using POBN as a spin trapping agent, as the characteristic EPR spectrum of •POBN-OH (a_N = 1.50 mT, $a_H{}^{\beta}$ = 0.165 mT, $a_{13C}(4 \times {}^{13}C)$ = 0.45 mT; g = 2.0058) [9,20,65] was observed upon photoexcitation of titania in aqueous media (inset in Fig. 3b). It should be noted here that these paramagnetic species may also be formed *via* an alternative reaction pathway including direct oxidation of DMPO or POBN by the photogenerated hole to the corresponding radical cation, followed by its hydrolysis to •DMPO-OH or •POBN-OH [15,20,66]. Fig. 2a and b shows the concentration of •DMPO-OH and •POBN-OH spin-adducts measured upon irradiation of aerated aqueous suspensions of samples **TC**350–**TC**750. The dependence of •DMPO-OH and •POBN-OH concentration upon UVA exposure was fitted by a non-linear least-squares method to the formal kinetic models, i.e., first-order or consecutive first-order kinetics when a decrease of spin-adduct concentration upon exposure was observed (Fig. 2a and b), subsequently the initial rates of photoinduced spin-adduct formation were calculated (R_{in}(•DMPO-OH) and R_{in}(•POBN-OH)), and finally the values of UVA photonic efficiencies of hydroxyl radical spin-adducts were determined using Eq. (4). Fig. 3a and b summarizes the obtained UVA photonic efficiencies of •DMPO-OH and •POBN-OH for mechanochemically synthesized titania samples **TC** and **TCSM**. The highest photonic efficiencies in the generation of hydroxyl radical spin-adducts, ξ_{UVA}(•DMPO-OH) and ξ_{UVA}(•POBN-OH), were found for samples **TC**650 and **TC**550 (Fig. 3a and b); generally, lower values were found for samples **TCSM** synthesized in the presence of a sulfate matrix. It is highly remarkable that the crystallization temperature of the non-crystalline network of hydrated TiO_2, at which anatase nanocrystals with optimal size for photocatalytic activity ~30–50 nm are formed, decreases in the presence of solely NH_4Cl salt matrix to 550–650 °C.

In analogy with our previous work [41], we propose that isometric nanocrystallites are evolved by annealing at 450 °C. It can be expected that their faceting coupled with high photoactivity occurred predominantly during calcination at temperatures of 550 and 650 °C. Further increase of annealing temperature caused growth of nanocrystallites above their optimal size for photoactivity (23–50 nm), as well as to development of rutile admixture (Table 1).

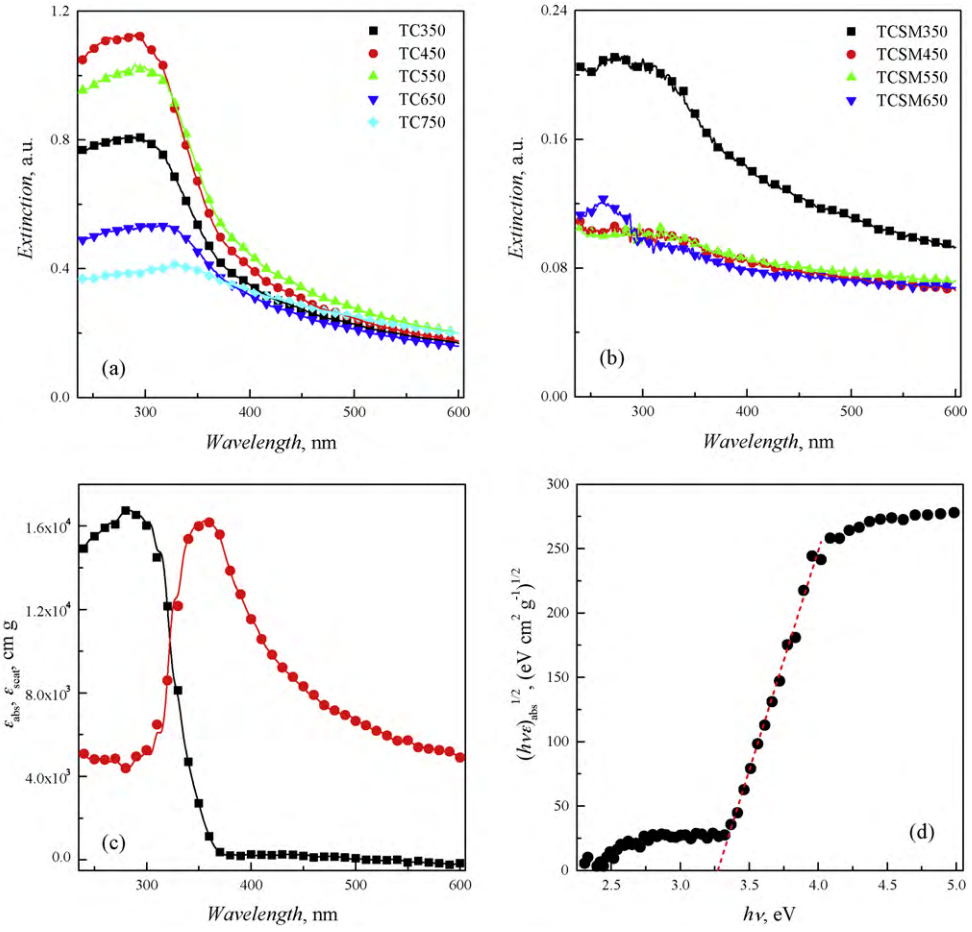

Fig. 1. (**a** and **b**) UV/vis extinction (absorption and scattering) spectra measured in aqueous suspensions of titania samples synthesized in the series **TC** and **TCSM** (TiO_2 concentration 4×10^{-5} g cm^{-3}). **(c)** The dependence of absorption (■) and scattering (●) coefficients on wavelength calculated for the **TC**550 sample. **(d)** The dependence of $(\varepsilon^{\lambda}_{abs}\, h\nu)^{1/2}$ on the photon energy (in eV) used in the evaluation of the TiO_2 band-gap energy for the sample **TC**550. The symbols represent the calculated values using the Kubelka–Munk model [39,41] and the dotted line was obtained by linear regression analysis assuming indirect transitions [61].

3.2.2. Termination of TEMPOL and ABTS$^{\bullet+}$

Previously, semi-stable nitroxide free radicals have been successfully applied as spin probes in the detection of reactive oxygen species and carbon-centered free radicals produced in various photochemical and biological systems [15,19,20,67–71]. This detection technique is based on the decrease of EPR signal intensity caused by the interaction of the nitroxide >N–O$^{\bullet}$ group with the reactive radical species resulting in the production diamagnetic products [19,20,72].

The nitroxide radical TEMPOL, characterized in aqueous media by a three-line EPR spectrum ($a_N = 1.70$ mT; $g = 2.0060$; inset in Fig. 3c), revealed sufficient stability under the given experimental conditions, since only a negligible decline of its concentration was observed during the photoexcitation of TiO_2-free solutions. On the other hand, irradiation of TEMPOL in aerated aqueous TiO_2 suspensions resulted in an exponential concentration decrease as shown in Fig. 2c for samples **TC**350–**TC**750. The initial rates of the photoinduced termination of TEMPOL (R_{in}(TEMPOL)) were calculated using least squares analysis, followed by the evaluation of photonic efficiencies of this process, ξ_{UVA}(TEMPOL), as is summarized in Fig. 3c. Surprisingly, high values of ξ_{UVA}(TEMPOL) were found for the amorphous samples **TC**150 and **TC**200, which contain the residual NH_4Cl from mechanochemical synthesis, consequently we assume that reactive nitrogen species, produced from ammonium ions upon TiO_2 photoexcitation (e.g., $^{\bullet}NO_2$), contributed to the termination of the nitroxide moiety of TEMPOL [73,74]. Among the crystalline **TC** titania powders a high ability to terminate TEMPOL was found for samples **TC**550 and **TC**650. On the other hand, ξ_{UVA}(TEMPOL) obtained in the **TCSM** series gradually decreased upon increase of annealing temperature (Fig. 3c), and the highest values were obtained for sample **TCSM**350.

The paramagnetic radical cation ABTS$^{\bullet+}$ (which gives a high-resolved EPR spectrum shown in inset of Fig. 3d) behaves as an effective scavenger of photogenerated electrons producing the diamagnetic ABTS molecule upon exposure in aerated aqueous TiO_2 suspensions [20,41]. Previously, the photoinduced electron transfer reaction ABTS$^{\bullet+}$/ABTS in TiO_2 suspensions has been monitored by the UV/vis spectroscopy, demonstrating a decrease of the ABTS$^{\bullet+}$ selective absorption bands at 735 and 415 nm, accompanied by a simultaneous growth of the ABTS absorption at 340 nm, with an isosbestic point at 368 nm [20,41]. Our *in situ* EPR experiments using mechanochemically synthesized titania powders confirmed a rapid decrease of ABTS$^{\bullet+}$ concentration under the given experimental conditions as shown in Fig. 2d for samples **TC**350–**TC**750. The calculated values of the photonic efficiencies of radical cation ABTS$^{\bullet+}$ reduction, ξ_{UVA}(ABTS$^{\bullet+}$) are summarized in Fig. 3d, and evidenced the high photoinduced activities of the titania samples **TC**450–**TC**650 and **TCSM**550.

3.2.3. TMP oxidation monitored by in situ EPR

The proposed reaction pathway of $^1O_2$ production upon photoexcitation of titanium dioxide included an electron transfer mechanism representing the formation of super oxide radical anions *via* reaction of molecular oxygen with photogenerated elec-

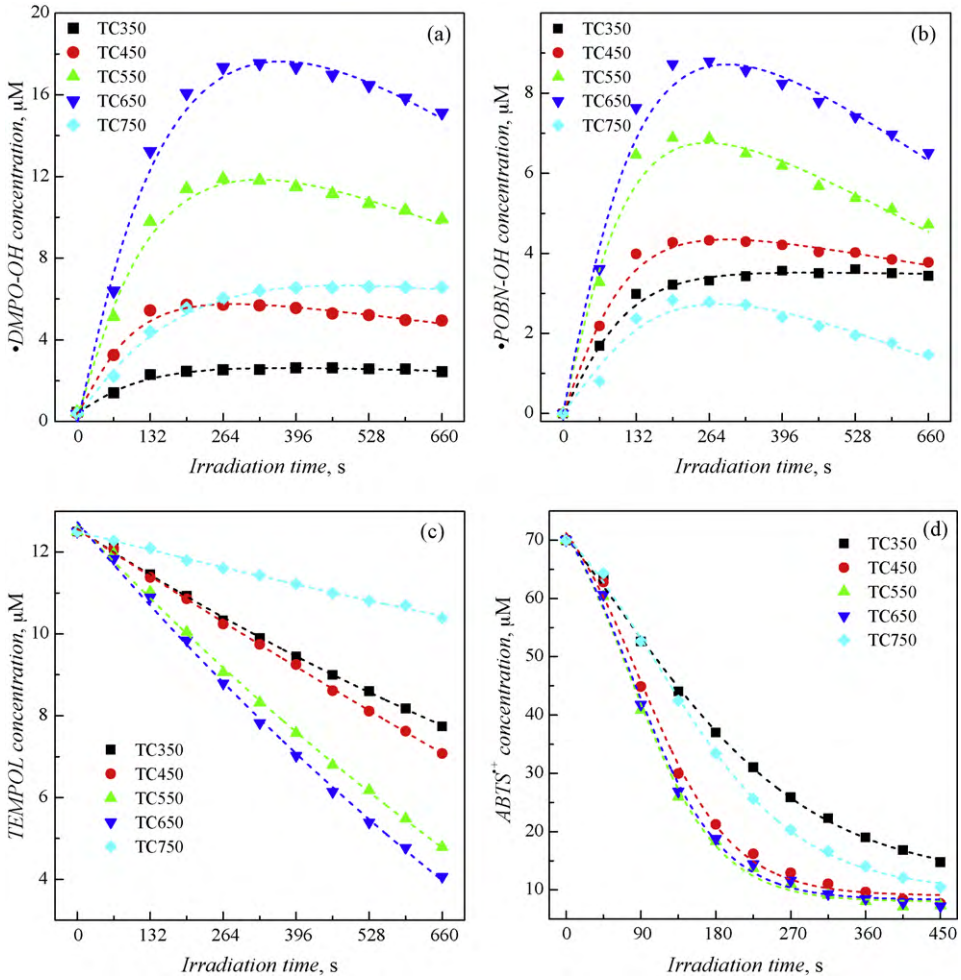

Fig. 2. Dependence of the paramagnetic species concentration on the irradiation time in aerated aqueous suspensions of synthesized TiO_2 samples (concentration 5×10^{-4} g cm^{-3}; ■ **TC**350; ● **TC**450; ▲ **TC**550; ▼ **TC**650; ◆ **TC**750): **(a)** •DMPO-OH (initial DMPO concentration $c_{0,DMPO}$ = 0.03 M); **(b)** •POBN-OH ($c_{0,POBN}$ = 0.03 M); **(c)** TEMPOL ($c_{0,TEMPOL}$ = 12.5 μM); **(d)** ABTS$^{\bullet+}$ ($c_{0,ABTS^{\bullet+}}$ = 70 μM). The symbols represent the experimental data and the dashed lines their mathematical simulations using least squares analysis.

trons, and consecutive oxidation of $O_2^{\bullet-}$ with photogenerated holes generating singlet oxygen [75,76]. The formation of singlet oxygen in photoexcited TiO_2 suspensions has been monitored by EPR using oxidation of sterically hindered cyclic amines to nitroxide radicals [23] and phosphorescence [75,76]. Previously, Nosaka et al. investigated using EPR the details of oxidation mechanism of TMP in the irradiated aqueous titania suspensions monitoring the effect of additives (DABCO, methanol, H_2O_2, SCN^-, I^-) on the initial rate of TEMPOL formation [77]. The results established that in aqueous media is TMP oxidized to nitroxide radicals by the photogenerated holes followed by the reaction with molecular oxygen, and the reactions of TMP with singlet oxygen, superoxide radical anions and hydroxyl radicals were excluded [77]. The electrochemical measurements evidenced additionally that under given experimental conditions in aqueous media the redox potential of TMP allows direct electron transfer between adsorbed TMP molecules and photogenerated holes [77].

Our attempts to evidence the photoinduced oxidation of TMP to paramagnetic TEMPOL were unsuccessful in H_2O or D_2O under the given experimental conditions probably because, in the aqueous TiO_2 suspensions, the photogenerated nitroxide radical TEMPOL is immediately scavenged by ROS produced simultaneously [67–71], or the concentration of TMP adsorbed on TiO_2 surface was too low, as the TiO_2 suspensions containing TMP were prepared immediately before EPR measurements.

Acetonitrile is, due to the higher solubility of molecular oxygen and the satisfactory lifetime of singlet oxygen, an appropriate solvent to monitor the generation of $^1O_2$ [78]. Additionally, acetonitrile as aprotic solvent may stabilize the super oxide radical anions generated in the photoexcited titania suspensions. The continuous UVA exposure of aerated acetonitrile TiO_2 suspensions of Aeroxide® P25 resulted in the progressive growth of a three-line EPR signal attributable to TEMPOL (a_N = 1.568 mT; g = 2.0060), as shown in Fig. 4a. Significant decrease of photogenerated TEMPOL concentration was monitored after addition of sodium azide as a selective singlet oxygen quencher into TiO_2 suspensions. Analogous EPR results were found recently upon irradiation of fluoroquinolone photosentitizers in the homogeneous acetonitrile solutions in the presence TMP [78]. The irradiation of TMP in TiO_2 suspensions prepared in mixed solvent acetonitrile:methanol(1:1; vol/vol) caused inhibition of TEMPOL formation, as methanol acts as effective photogenerated hole scavenger producing hydroxymethyl radicals [79], and additionally can influence $^1O_2$ lifetime [80].

The comparable behaviour of TMP oxidation to nitroxide radical TEMPOL in the particulate acetonitrile TiO_2 suspensions and in homogeneous photoexcited solutions containing fluoroquinolones, as well as the quenching effects of sodium azide in both systems [78] may evoke that TMP is oxidized by singlet oxygen [81]. However, the reaction mechanism proposed by Nosaka for oxidation of

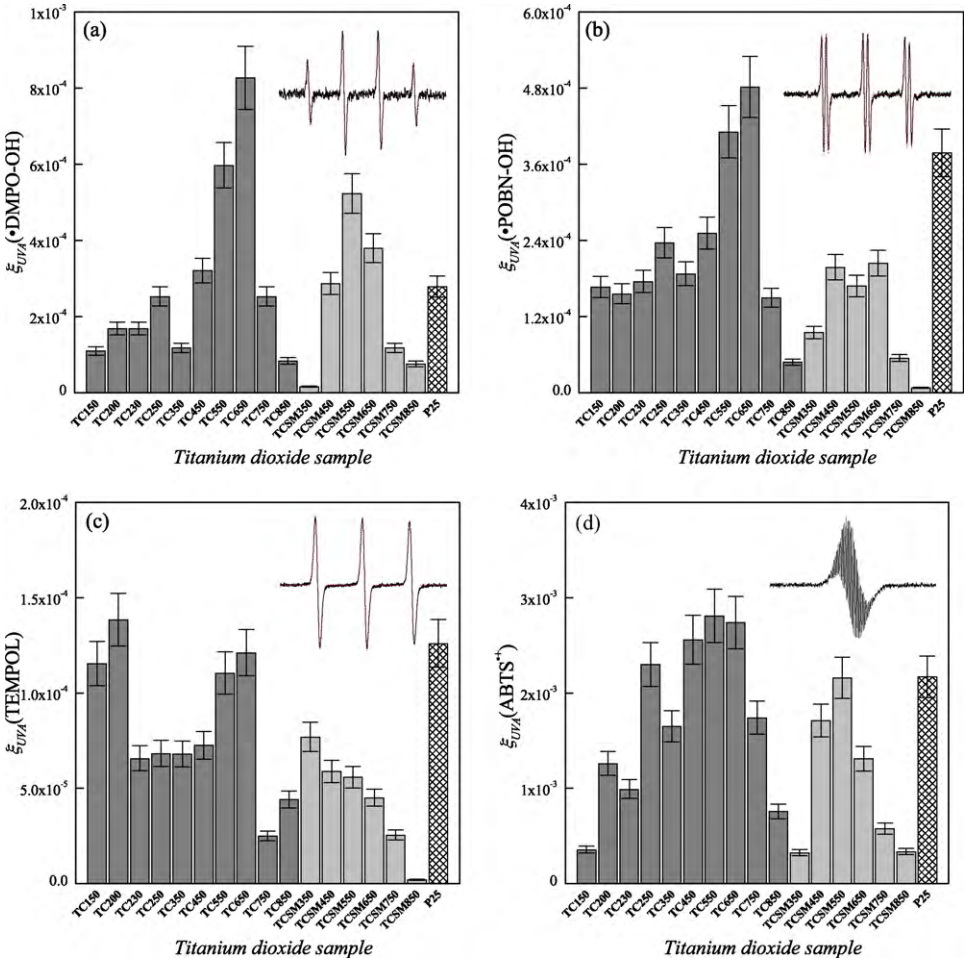

Fig. 3. Values of the UVA photonic efficiency determined using EPR spectroscopy in aerated aqueous suspensions of mechanochemically synthesized titanium dioxide powders **TC**, **TCSM**, along with Aeroxide® P25, monitoring the changes in concentration of the paramagnetic species: **(a)** •DMPO-OH; inset represents experimental (solid line) and simulated (dashed line) EPR spectrum of •DMPO-OH (SW = 7 mT); **(b)** •POBN-OH; inset shows the experimental (solid line) and simulated (dashed line) EPR spectrum of •POBN-OH (SW = 6 mT); **(c)** TEMPOL; inset illustrates the experimental (solid line) and simulated (dashed line) EPR spectrum of •TEMPOL (SW = 6 mT), and **(d)** ABTS•+; inset represents high-resolved EPR spectrum of ABTS•+ (SW = 10 mT).

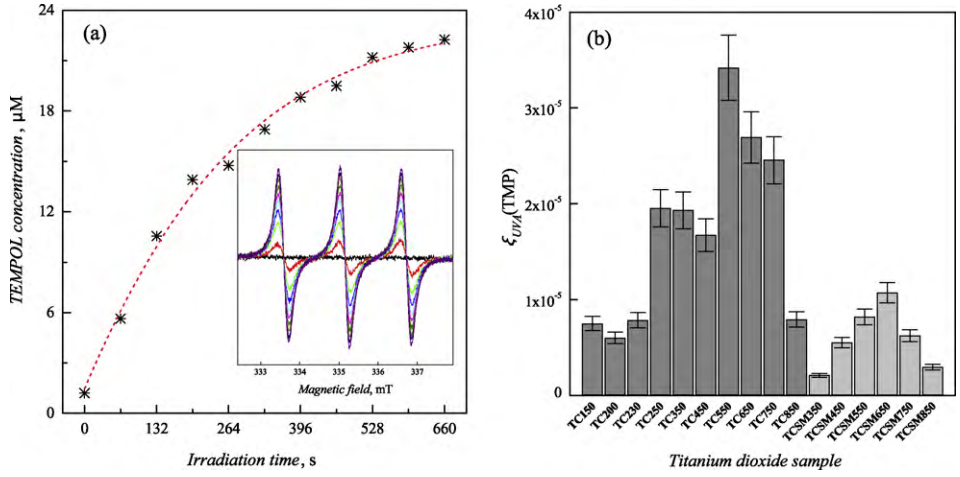

Fig. 4. **(a)** Dependence of the concentration of TEMPOL (produced *via* oxidation of TMP) upon irradiation time in aerated acetonitrile suspensions of Aeroxide® P25 (concentration 5×10^{-4} g cm^{-3}; initial TMP concentration $c_{0,TMP}$ = 0.01 M). The symbols represent the experimental data and dashed lines their mathematical simulations using least squares analysis. Inset shows the time-course of EPR spectra monitored in the experimental system (the first spectrum (–) was measured without irradiation; the time interval between EPR spectra is 66 s). **(b)** Values of the UVA photonic efficiency determined using EPR spectroscopy in aerated acetonitrile suspensions of mechanochemically synthesized titanium dioxide powders **TC** and **TCSM** monitoring the concentration increase of TEMPOL (produced *via* oxidation of TMP).

Table 2
The correlation coefficient values calculated between the photonic efficiencies determined with EPR spectroscopy monitoring formation of spin-adducts •DMPO-OH and •POBN-OH, disappearance of paramagnetic species TEMPOL and $ABTS^{\bullet+}$, or oxidation of TMP, found by the investigation of mechanochemically synthesized titanium dioxide powders.

	•DMPO-OH	•POBN-OH	TEMPOL	$ABTS^{\bullet+}$	TMP
•DMPO-OH	1				
•POBN-OH	0.8748	1			
TEMPOL	0.6560	0.8707	1		
$ABTS^{\bullet+}$	0.8115	0.8653	0.6710	1	
TMP	0.6464	0.7960	0.5910	0.8021	1

TMP in aqueous TiO_2 systems [77], represents an alternative reaction pathway, taking into account the effect of acetonitrile solvent on redox potentials of TMP and photogenerated holes [1,2].

The values of photonic efficiency calculated from the initial rate of TMP oxidation, ξ_{UVA}(TMP), summarized in Fig. 4b, were used to compare photoactivity of mechanochemically synthesized titania nanopowders. It should be noted here that $\xi_{UVA}(TMP) = 3 \times 10^{-4}$ found for the Aeroxide® P25 sample significantly exceeded the values obtained for mechanochemically synthesized titania nanopowders ($\xi_{UVA}(TMP) < 4 \times 10^{-5}$; Fig. 4b) although comparable photoactivities were found using agents DMPO, POBN, TEMPOL and $ABTS^{\bullet+}$ (Fig. 3). Previously, the high photoactivity of P25 has been attributed to either the efficient separation of the electron–hole pairs or to the inhibition of their recombination and these effects have been explained by considering synergetic effects between anatase and rutile nanoparticles [82,83].

3.2.4. Mutual correlation between the photonic efficiencies found by EPR

Previously, spin trapping agents and nitroxide radicals as spin probes have been successfully applied to the indirect detection of hydroxyl radical formation upon TiO_2 irradiation, assuming detection of adsorbed •OH or trapped holes produced on irradiated surface [15]. However, these results evidenced no correlation with experimental data obtained by hydroxyl radicals quantified *via* fluorescence detection using hydroxylation of terephthalic acid, demonstrating that fluorescence can detect hydroxyl radicals in bulk solution, on the contrary photogenerated surface hydroxyl radicals monitored by EPR [15].

In order to evaluate linear relationships between data obtained by various EPR techniques we calculated the correlation between couples of photonic efficiencies, and the obtained correlation coefficients characterize the strength of association between two variables under consideration. According to Cohen's definition the value of correlation coefficient over 0.5 represents large correlation [84].

In our investigations mutual linear correlations between all couples of photonic efficiencies were determined for 14 mechanochemically synthesized TiO_2 samples (amorphous **TC**150 and **TC**200 were omitted due to the presence of residual NH_4Cl). In spite of the complexity of photoinduced processes monitored by EPR spectroscopy in heterogeneous titania systems, large correlations were found, characterized with correlation coefficients in the range of 0.5910–0.8748 (Table 2). As between all couples of photonic efficiencies linear correlation was found, we may presuppose that radicals monitored in our study using EPR upon *in situ* photoexcitation of titania (•DMPO-OH, •POBN-OH, TEMPOL, $ABTS^{\bullet+}$) are formed or quenched with photogenerated species produced on the titania surface, and each of presented experimental EPR technique can be applied in characterization of TiO_2 photoactivity.

4. Conclusions

Mechanochemical synthesis using liquid $TiCl_4$ and $(NH_4)_2CO_3$, with a post-milling annealing process in the temperature range of 150–850 °C represents a simple method for the synthesis of TiO_2 nanopowders characterized with controlled nanoparticle size and photoactivity. The presence of a salt matrix plays an important role in the process of anatase nanocrystallites growth, influencing significantly their size, surface properties and crystallization temperature. Using $TiCl_4/(NH_4)_2CO_3$ in a molar ratio 1:3 (series **TC**), the nanocrystalline anatase was formed even at a temperature of 250 °C, about 100 °C lower as usually found for solid state synthesis of nanocrystals, and this effect was attributed to either the presence of the salt matrix NH_4Cl or its decomposition products (HCl and NH_3). For series **TC**, annealing temperatures of 550 and 650 °C resulted in the formation of anatase particles with a mean crystallite size of 31 and 50 nm, respectively, possessing the highest activities in the photoinduced production of ROS. On the other hand, in series **TCSM** mechanochemically synthesized from $TiCl_4/(NH_4)_2CO_3$ (molar ratio 1:2) with the addition of sulfates, the development of anatase nanocrystals was evidenced at 350 °C, since the presence of sulfate salt matrix significantly hindered TiO_2 nanocrystallites growth, increased agglomerate formation in aqueous media and lowered the values of photonic efficiencies determined by EPR spectroscopy using various experimental techniques.

Acknowledgements

The authors wish to thank to Scientific Grant Agency of the Slovak Republic (Projects VEGA/1/0018/09, VEGA/1/0337/08, VEGA/1/0162/10, VEGA 2/0160/10) and to the Science and Technology Assistance Agency Slovakia (project APVV-VVCE-003307) for financial support. This work was also supported by Agency of the Ministry of Education of the Slovak Republic for the Structural Funds of the EU, Operational Programme Research and Development (OPVaV-2008/4.1/01-SORO), Project Code 262 401 200 11 and (OPVaV-2009/4.1/02-SORO), Project Code 262 401 200 19. Dušana Mocinecová is acknowledged for technical assistance and Harry Morris for helpful discussion.

References

[1] P. Kamat, Chem. Rev. 93 (1993) 267–300.
[2] M. Hoffmann, S. Martin, W. Choi, D. Bahnemann, Chem. Rev. 95 (1995) 69–96.
[3] O. Carp, C. Huisman, A. Reller, Prog. Solid State Chem. 32 (2004) 33–177.
[4] U. Gaya, A. Abdullah, J. Photochem. Photobiol. C 9 (2008) 1–12.
[5] A. Mills, S. LeHunte, J. Photochem. Photobiol. A 108 (1997) 1–35.
[6] A. Testino, I. Bellobono, V. Buscaglia, C. Canevali, M. D'Arienzo, S. Polizzi, R. Scotti, F. Morazzoni, J. Am. Chem. Soc. 129 (2007) 3564–3575.
[7] D. Bahnemann, M. Hilgendorff, R. Memming, J. Phys. Chem. B 101 (1997) 4265–4275.
[8] M. Abellan, R. Dillert, J. Gimenez, D. Bahnemann, J. Photochem. Photobiol. A 202 (2009) 164–171.
[9] R. Scotti, M. D'Arienzo, A. Testino, F. Morazzoni, Appl. Catal. B 88 (2009) 497–504.
[10] R. Scotti, I. Bellobono, C. Canevali, C. Cannas, M. Catti, M. D'Arienzo, A. Musinu, S. Polizzi, M. Sommariva, A. Testino, F. Morazzoni, Chem. Mater. 20 (2008) 4051–4061.
[11] J. Zhang, Q. Xu, Z. Feng, M. Li, C. Li, Angew. Chem. Int. Ed. 47 (2008) 1766–1769.
[12] L. Sun, J. Bolton, J. Phys. Chem. 100 (1996) 4127–4134.
[13] K. Ishibashi, A. Fujishima, T. Watanabe, K. Hashimoto, Electrochem. Commun. 2 (2000) 207–210.
[14] T. Hirakawa, C. Koga, N. Negishi, K. Takeuchi, S. Matsuzawa, Appl. Catal. B 87 (2009) 46–55.
[15] Y. Nosaka, S. Komori, K. Yawata, T. Hirakawa, A. Nosaka, Phys. Chem. Chem. Phys. 5 (2003) 4731–4735.
[16] T. Uchino, H. Tokunaga, M. Ando, H. Utsumi, Toxicol. In Vitro 16 (2002) 629–635.
[17] T. Hirakawa, T. Daimon, M. Kitazawa, N. Ohguri, C. Koga, N. Negishi, S. Matsuzawa, Y. Nosaka, J. Photochem. Photobiol. A 190 (2007) 58–68.
[18] D. Dvoranová, V. Brezová, M. Mazúr, M. Malati, Appl. Catal. B 37 (2002) 91–105.
[19] V. Brezová, S. Gabčová, D. Dvoranová, A. Staško, J. Photochem. Photobiol. B 79 (2005) 121–134.

[20] V. Brezová, D. Dvoranová, A. Staško, Res. Chem. Intermed. 33 (2007) 251–268.
[21] C.D. Jaeger, A.J. Bard, J. Phys. Chem. 83 (1979) 3146–3152.
[22] E. Carter, A. Carley, D. Murphy, J. Phys. Chem. C 111 (2007) 10630–10638.
[23] R. Konaka, E. Kasahara, W. Dunlap, Y. Yamamoto, K. Chien, M. Inoue, Free Radical Biol. Med. 27 (1999) 294–300.
[24] S. Bakardjieva, V. Štengl, L. Szatmary, J. Šubrt, J. Lukáč, N. Murafa, D. Nižnánsky, K. Čižek, J. Jirkovský, N. Petrova, J. Mater. Chem. 16 (2006) 1709–1716.
[25] C. Cho, D. Kim, D. Kim, J. Am. Ceram. Soc. 86 (2003) 1138–1145.
[26] C. Cho, M. Han, D. Kim, D. Kim, Mater. Chem. Phys. 92 (2005) 104–111.
[27] G. Lee, H. Zuo, J. Am. Ceram. Soc. 87 (2004) 473–479.
[28] G. Colon, M. Hidalgo, G. Munuera, I. Ferino, M. Cutrufello, J. Navio, Appl. Catal. B 63 (2006) 45–59.
[29] J. Wu, S. Hao, J. Lin, M. Huang, Y. Huang, Z. Lan, P. Li, Cryst. Growth Des. 8 (2008) 247–252.
[30] P. Billik, G. Plesch, Mater. Lett. 61 (2007) 1183–1186.
[31] P. Billik, G. Plesch, Scr. Mater. 56 (2007) 979–982.
[32] P. Billik, G. Plesch, V. Brezová, Ľ. Kuchta, Valko M., Mazúr M., J. Chem. Phys. Solids 68 (2007) 1112–1116.
[33] A. Dodd, A. McKinley, T. Tsuzuki, M. Saunders, J. Chem. Phys. Solids 68 (2007) 2341–2348.
[34] M. Salari, M. Rezaee, S. Marashi, S. Aboutalebi, Powder Technol. 192 (2009) 54–57.
[35] M. Salari, S. Khoie, P. Marashi, M. Rezaee, J. Alloys Compd. 469 (2009) 386–390.
[36] P. Billik, M. Čaplovičová, Ľ. Čaplovič, Mater. Res. Bull. 45 (2010) 621–627.
[37] R. Smith, G. Rohrer, A. Perrotta, J. Am. Ceram. Soc. 84 (2001) 1896–1902.
[38] H. Zhang, J.F. Banfield, J. Phys. Chem. B 104 (2000) 3481–3487.
[39] D. Vione, C. Minero, V. Maurino, A. Carlotti, T. Picatonotto, E. Pelizzetti, Appl. Catal. B 58 (2005) 79–88.
[40] L. McNeil, R. French, Acta Mater. 48 (2000) 4571–4576.
[41] V. Brezová, Z. Vrecková, P. Billik, M. Čaplovičová, G. Plesch, J. Photochem. Photobiol. A 206 (2009) 177–187.
[42] S. Jantová, S. Letašiová, V. Brezová, Ľ. Čipák, J. Lábaj, J. Photochem. Photobiol. B 85 (2006) 163–176.
[43] WinSIM, NIEHS, Research Triangle Park, NC, USA, 2002.
[44] Hari-Bala, Y. Guo, X. Zhao, J. Zhao, W. Fu, X. Ding, Y. Jiang, K. Yu, X. Lv, Z. Wang, Mater. Lett. 60 (2006) 494–498.
[45] R.K. Wahi, Y. Liu, J.C. Falkner, V.L. Colvin, J. Colloid Interf. Sci. 302 (2006) 530–536.
[46] H. Yin, Y. Wada, T. Kitamura, S. Kambe, S. Murasawa, H. Mori, T. Sakata, S. Yanagida, J. Mater. Chem. 11 (2001) 1694–1703.
[47] B. Chen, H. Zhang, B. Gilbert, J. Banfield, Phys. Rev. Lett. 98 (2007), art. no. 106103.
[48] J. Zhang, M. Li, Z. Feng, J. Chen, C. Li, J. Phys. Chem. B 110 (2006) 927–935.
[49] X. Bokhimi, A. Morales, E. Ortiz, T. Lopez, R. Gomez, J. Navarrete, J. Sol–Gel Sci. Technol. 29 (2004) 31–40.
[50] J. Sohn, S. Lee, P. Cheon, H. Kim, Bull. Korean Chem. Soc. 25 (2004) 657–664.
[51] Y. Kolen'ko, A. Burukhin, B. Churagulov, N. Oleinikov, Inorg. Mater. 40 (2004) 822–828.
[52] V. Gun'ko, J. Blitz, V. Zarko, V. Turov, E. Pakhlov, O. Oranska, E. Goncharuk, Y. Gornikov, V. Sergeev, T. Kulik, B. Palyanytsya, R. Samala, J. Colloid Interf. Sci. 330 (2009) 125–137.
[53] F. Lonyi, J. Valyon, J. Therm. Anal. 46 (1996) 211–218.
[54] M. Cabrera, O. Alfano, A. Cassano, J. Phys. Chem. 100 (1996) 20043–20050.
[55] U. Gesenhues, Chem. Eng. Technol. 24 (2001) 685–694.
[56] I. Martyanov, E. Savinov, K. Klabunde, J. Colloid Interf. Sci. 267 (2003) 111–116.
[57] Q. Zhang, L. Gao, J. Eur. Ceram. Soc. 26 (2006) 1535–1545.
[58] J. Marugan, R. Van Grieken, O. Alfano, A. Cassano, AICHE J. 52 (2006) 2832–2843.
[59] S. Yurdakal, V. Loddo, B. Ferrer, G. Palmisano, V. Augugliaro, J. Farreras, L. Palmisano, Ind. Eng. Chem. Res. 46 (2007) 7620–7626.
[60] M. Mikula, M. Čeppan, J. Kindernay, D. Búc, Czech. J. Phys. 49 (1999) 393–403.
[61] K. Reddy, S. Manorama, A. Reddy, Mater. Chem. Phys. 78 (2003) 239–245.
[62] Y. Du, J. Rabani, J. Phys. Chem. B 107 (2003) 11970–11978.
[63] N. Serpone, A. Salinaro, Pure Appl. Chem. 71 (1999) 303–320.
[64] J. Marugan, D. Hufschmidt, G. Sagawe, V. Selzer, D. Bahnemann, Water Res. 40 (2006) 833–839.
[65] A. Li, K. Cummings, H. Roethling, G. Buettner, C. Chignell, J. Magn. Reson. 79 (1988) 140–142.
[66] L. Eberson, Acta Chem. Scand. 53 (1999) 584–593.
[67] S. Goldstein, A. Samuni, J. Phys. Chem. A 111 (2007) 1066–1072.
[68] A. Samuni, S. Goldstein, A. Russo, J. Mitchell, M. Krishna, P. Neta, J. Am. Chem. Soc. 124 (2002) 8719–8724.
[69] E. Damiani, R. Castagna, L. Greci, Free Radical Biol. Med. 33 (2002) 128–136.
[70] P. Schwarz, N. Turro, S. Bossmann, A. Braun, A. Wahab, H. Durr, J. Phys. Chem. B 101 (1997) 7127–7134.
[71] K. Takeshita, K. Saito, J. Ueda, K. Anzai, T. Ozawa, Biochim. Biophys. Acta: Gen. Subj. 1573 (2002) 156–164.
[72] K.D. Asmus, S. Nigam, R.L. Willson, Int. J. Radiat. Biol. 29 (1976) 211–219.
[73] S. Goldstein, A. Samuni, A. Russo, J. Am. Chem. Soc. 125 (2003) 8364–8370.
[74] S. Goldstein, A. Samuni, G. Merenyi, Chem. Res. Toxicol. 17 (2004) 250–257.
[75] T. Daimon, T. Hirakawa, M. Kitazawa, J. Suetake, Y. Nosaka, Appl. Catal. A 340 (2008) 169–175.
[76] T. Daimon, T. Hirakawa, Y. Nosaka, Electrochemistry 76 (2008) 136–139.
[77] Y. Nosaka, H. Natsui, M. Sasagawa, A. Nosaka, J. Phys. Chem. B 110 (2006) 12993–12999.
[78] J. Rimarčík, V. Lukeš, E. Klein, A.-M. Kelterer, V. Milata, Z. Vrecková, V. Brezová, J. Photochem. Photobiol. A 211 (2010) 47–58.
[79] V. Brezová, P. Tarábek, D. Dvoranová, A. Staško, S. Biskupič, J. Photochem. Photobiol. A 155 (2003) 179–198.
[80] A. Braun, E. Oliveros, Pure Appl. Chem. 62 (1990) 1467–1476.
[81] L. Zang, F. vanKuijk, B. Misra, H. Misra, Biochem. Mol. Biol. Int. 37 (1995) 283–293.
[82] K. Baiju, A. Zachariah, S. Shukla, S. Biju, M. Reddy, K. Warrier, Catal. Lett. 130 (2009) 130–136.
[83] A. Zachariah, K. Baiju, S. Shukla, K. Deepa, J. James, K. Warrier, J. Phys. Chem. C 112 (2008) 11345–11356.
[84] J. Cohen, Statistical Power Analysis for the Behavioral Sciences, second ed., Lawrence Erlbaum, New Jersey, 1988.